ROBUST WEIGHT INITIALIZATION FOR TANH NEURAL NETWORKS WITH FIXED POINT ANALYSIS

Hyunwoo Lee[1], **Hayoung Choi**[1*], **Hyunju Kim**[2*]
[1]Kyungpook National University, [2]Korea Institute of Energy Technology
[1]{lhw908, hayoung.choi}@knu.ac.kr, [2]hjkim@kentech.ac.kr

ABSTRACT

As a neural network's depth increases, it can achieve high generalization performance. However, training deep networks is challenging due to gradient and signal propagation issues. To address these challenges, extensive theoretical research and various methods have been introduced. Despite these advances, effective weight initialization methods for tanh neural networks remain underexplored. This paper presents a novel weight initialization method for neural networks with tanh activation function. Based on an analysis of the fixed points of the function $\tanh(ax)$, the proposed method aims to determine values of a that mitigate activation saturation. A series of experiments on various classification datasets and physics-informed neural networks demonstrates that the proposed method outperforms Xavier initialization methods (with or without normalization) in terms of robustness across different network sizes, data efficiency, and convergence speed. Code is available at `https://github.com/1HyunwooLee/Tanh-Init`.

1 INTRODUCTION

Deep learning has significantly advanced state-of-the-art performance across various domains (LeCun et al., 2015; He et al., 2016). The expressivity of neural networks increases exponentially with depth, enhancing generalization performance (Poole et al., 2016; Raghu et al., 2017). However, deeper networks often face gradient and signal propagation issues (Bengio et al., 1993). These challenges have driven the development of effective weight initialization methods designed for various activation functions. Xavier initialization (Glorot & Bengio, 2010) prevents saturation in sigmoid and tanh activations, while He initialization (He et al., 2015) stabilizes variance for ReLU networks. Especially in ReLU neural networks, several weight initialization methods have been proposed to mitigate the dying ReLU problem, which hinders signal propagation in deep networks (Lu et al., 2019; Lee et al., 2024). However, to the best of our knowledge, research on initialization methods that are robust across different sizes of tanh networks remains underexplored. Tanh networks commonly employ Xavier initialization (Raissi et al., 2019; Jagtap et al., 2022; Rathore et al., 2024) and are widely applied in various domains, such as Physics-Informed Neural Networks (PINNs) (Raissi et al., 2019) and Recurrent Neural Networks (RNNs) (Rumelhart et al., 1986), with performance often dependent on model size and initialization randomness (Liu et al., 2022).

The main contribution of this paper is the proposal of a simple weight initialization method for FeedForward Neural Networks (FFNNs) with tanh activation function. The proposed method is data-efficient and demonstrates robustness across different network sizes. Moreover, it reduces dependency on normalization techniques such as Batch Normalization (BN) (Ioffe, 2015) and Layer Normalization (LN) (Ba, 2016). As a result, it alleviates the need for extensive hyperparameter tuning, such as selecting the number of hidden layers and units, while also eliminating the computational overhead associated with normalization. The theoretical foundation of this approach is based on the fixed point of the function $\tanh(ax)$. We evaluate the proposed method on two tasks: classification and PINNs. For classification tasks, we assess its performance across various FFNN sizes using standard benchmark datasets. The results demonstrate improved validation accuracy and lower loss compared to Xavier initialization with BN or LN. For PINNs, the method exhibits robustness across diverse network sizes and demonstrates its effectiveness in solving a wide range of PDE

*Corresponding authors.

problems. Notably, for both tasks, the proposed method outperforms Xavier initialization in data efficiency; that is, it achieves improved performance even with limited data. Our main contributions can be summarized as follows:

- We identify the conditions under which activation values do not vanish as the neural network depth increases, using a fixed-point analysis (Section 3.1 and 3.2).
- We propose a novel weight initialization method for tanh neural networks that is robust across different network sizes and demonstrates high data efficiency (Section 3.2 and 3.3).
- We experimentally show that the proposed method is more robust across different network sizes on image benchmarks and PINNs (Section 4).
- We experimentally show that the proposed method is more data-efficient than Xavier initialization, with or without normalization, on image benchmarks and PINNs (Section 4).

2 Related works

The expressivity of neural networks grows exponentially with depth, resulting in improved generalization performance (Poole et al., 2016; Raghu et al., 2017). Proper weight initialization is crucial for effectively training deep networks (Saxe et al., 2014; Mishkin & Matas, 2016). Xavier (Glorot & Bengio, 2010) and He He et al. (2015) initialization are common initialization methods typically used with tanh and ReLU activation functions, respectively. Several initialization methodss have been proposed to improve the training of deep ReLU networks (Lu et al., 2019; Bachlechner et al., 2021; Zhao et al., 2022; Lee et al., 2024). However, research on weight initialization for tanh-based neural networks remains relatively limited. Despite this, tanh networks have gained increasing attention in recent years, particularly in applications such as PINNs, where their performance is highly sensitive to initialization randomness.

PINNs have shown promising results in solving forward, inverse, and multiphysics problems in science and engineering. (Lu et al., 2021; Karniadakis et al., 2021; Cuomo et al., 2022; Yin et al., 2021; Wu et al., 2023; Hanna et al., 2022; Bararnia & Esmaeilpour, 2022; Shukla et al., 2020; Zhu et al., 2024; Hosseini et al., 2023; Mao et al., 2020). PINNs approximate solutions to partial differential equations (PDEs) using neural networks and are trained by minimizing a loss function, typically formulated as a sum of least-squares terms incorporating PDE residuals, boundary conditions, and initial conditions. This loss is commonly optimized using gradient-based methods such as Adam (Kingma & Ba, 2014), L-BFGS (Liu & Nocedal, 1989), or a combination of both. Universal approximation theorems (Cybenko, 1989; Hornik et al., 1989; Hornik, 1991; Park et al., 2021; Guliyev & Ismailov, 2018b; Shen et al., 2022; Guliyev & Ismailov, 2018a; Maiorov & Pinkus, 1999; Yarotsky, 2017; Gripenberg, 2003) establish the theoretical capability of neural networks to approximate analytic PDE solutions. However, PINNs still face challenges in accuracy, stability, computational complexity, and tuning optimal hyperparameters of loss terms.

To address these challenges, various enhanced versions of PINNs have been proposed: (1) Self-adaptive loss-balanced PINNs (lbPINNs), which automatically adjust the hyperparameters of loss terms during training (Xiang et al., 2022), (2) Bayesian PINNs (B-PINNs), designed to handle forward and inverse nonlinear problems with noisy data (Yang et al., 2021), (3) Rectified PINNs (RPINNs), which incorporate gradient information from numerical solutions obtained via the multigrid method and are specifically designed for solving stationary PDEs (Peng et al., 2022), (4) Auxiliary PINNs (A-PINNs), developed to effectively handle integro-differential equations (Yuan et al., 2022), (5) Conservative PINNs (cPINNs) and Extended PINNs (XPINNs), which employ domain decomposition techniques (Jagtap et al., 2020; Jagtap & Karniadakis, 2020), (6) Parallel PINNs, designed to reduce the computational cost of cPINNs and XPINNs (Shukla et al., 2021), and (7) Gradient-enhanced PINNs (gPINNs), which incorporate the gradient of the PDE loss term with respect to network inputs (Yu et al., 2022).

While these advancements address various challenges in PINNs, activation functions and their initialization strategies remain crucial for achieving optimal performance.The tanh activation function has been shown to perform well in PINNs (Raissi et al., 2019), as detailed experimental results in Appendix C.2. Xavier initialization is widely employed as the standard approach for tanh networks in existing studies (Jin et al., 2021; Son et al., 2023; Yao et al., 2023; Gnanasambandam et al., 2023; Song et al., 2024). However, our experimental results indicate that employing Xavier initialization

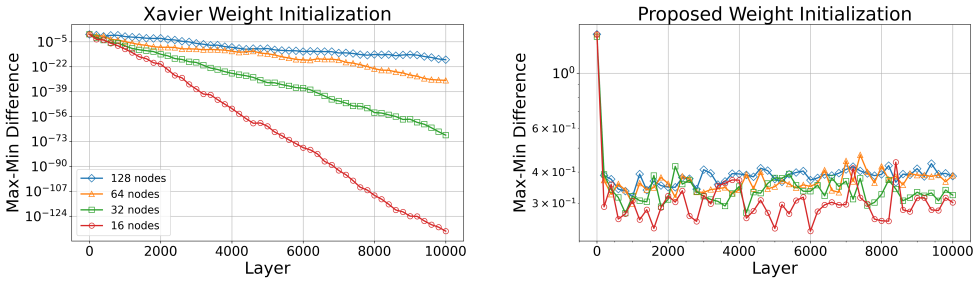

(a) Xavier Initialization

(b) Proposed Initialization

Figure 1: Difference between the maximum and minimum activation values at each layer when propagating $3,000$ input samples through a $10,000$-layer tanh FFNN, using Xavier initialization **(left)** and the proposed initialization **(right)**. Experiments were conducted on distinct networks with $10,000$ hidden layers, each having the same number of nodes: 16, 32, 64, or 128.

leads to decreased model performance as network size increases. Moreover, performance gains from Batch Normalization or Layer Normalization remain limited, and the method exhibits sensitivity to the amount of training data, particularly in smaller datasets. Although a recent study has proposed an initialization method for PINNs, it relies on transfer learning (Tarbiyati & Nemati Saray, 2023). To address these limitations, we propose a weight initialization method that is robust across different network sizes, achieves high data efficiency, and reduces reliance on both transfer learning and normalization techniques.

3 Proposed Weight Initialization Method

In this section, we discuss the proposed weight initialization method. Section 3.1 introduces the theoretical motivation behind the method. Section 3.2 presents how to derive the initial weight matrix that satisfies the conditions outlined in Section 3.1. Finally, in Section 3.3, we suggest the optimal hyperparameter σ_z in the proposed method.

3.1 Theoretical Motivation

Experimental results in Figure 1 indicate that when Xavier initialization is employed in FFNNs with tanh activation, the distribution of activation values tends to cluster around zero in deeper layers. This vanishing of activation values can hinder the training process due to a discrepancy between the activation values and the desired output. However, it is not straightforward to theoretically establish the conditions for preventing this phenomenon. In this section, we present a theoretical analysis based on a fixed point of $\tanh(ax)$ to mitigate this issue. Before giving the theoretical foundations, consider the basic results for a hyperbolic tangent activation function. Recall that if $f : \mathbb{R} \to \mathbb{R}$ is a function, then an element $x^* \in \mathbb{R}$ is called a *fixed point* of f if $f(x^*) = x^*$.

Lemma 1. *For a fixed $a > 0$ define the function $\phi_a : \mathbb{R} \to \mathbb{R}$ given as*

$$\phi_a(x) := \tanh(ax).$$

Then, there exists a fixed point x^* of ϕ_a. Furthermore,

(1) *if $0 < a \leq 1$, then ϕ_a has a unique fixed point $x^* = 0$.*

(2) *if $a > 1$, then ϕ_a has three distinct fixed points: $x^* = -\xi_a$, 0, ξ_a such that $\xi_a > 0$.*

Proof. The proof is detailed in Appendix A.1. □

Note that $\tanh(x) < x$ for all $x > 0$. However, according to Lemma 1, for $a > 1$ the behavior of $\tanh(ax)$ changes. If $x > \xi_a$ (resp. $x < \xi_a$), then $\tanh(ax) < x$ (resp. $\tanh(ax) > x$). At $x = \xi_a$, the equality $\tanh(ax) = x$ holds. The following lemma addresses the convergence properties of iteratively applying $\tanh(ax)$ for any $x > 0$.

Lemma 2. *For a given initial value $x_0 > 0$ define*

$$x_{n+1} = \phi_a(x_n), \quad n = 0, 1, 2, \ldots.$$

Then $\{x_n\}_{n=1}^{\infty}$ converges regardless of the positive initial value $x_0 > 0$. Moreover,

(1) *if $0 < a \leq 1$, then $x_n \to 0$ as $n \to \infty$.*

(2) *if $a > 1$, then $x_n \to \xi_a$ as $n \to \infty$.*

Proof. The proof is detailed in Appendix A.2. □

Note that for $a > 1$ and $x_0 > \xi_a > 0$, the sequence $\{x_n\}$ satisfies $\tanh(ax_n) > \tanh(ax_{n+1}) > \xi_a$ for all $n \in \mathbb{N}$. Similarly, when $0 < x_0 < \xi_a$, the sequence satisfies $\tanh(ax_n) < \tanh(ax_{n+1}) < \xi_a$ for all $n \in \mathbb{N}$. Given $a > 1$ and $x_0 < 0$, the sequence converges to $-\xi_a$ as $n \to \infty$ due to the odd symmetry of $\tanh(ax)$. According to Lemma 2, when $a > 1$, the sequence $\{x_n\}$ converges to ξ_a or $-\xi_a$, respectively, as $n \to \infty$, for an arbitrary initial value $x_0 > 0$ or $x_0 < 0$.

Note that the parameter a in Lemma 2 does not change across all iterations. Propositions 3 and Corollary 4, consider the case where the value of a varies for each iteration.

Proposition 3. *Let $\{a_n\}_{n=1}^{\infty}$ be a positive real sequence, i.e., $a_n > 0$ for all $n \in \mathbb{N}$, such that only finitely many elements are greater than 1. Suppose that $\{\Phi_m\}_{m=1}^{\infty}$ is a sequence of functions defined as for each $m \in \mathbb{N}$*

$$\Phi_m = \phi_{a_m} \circ \phi_{a_{m-1}} \circ \cdots \circ \phi_{a_1}.$$

Then for any $x \in \mathbb{R}$

$$\lim_{m \to \infty} \Phi_m(x) = 0.$$

Proof. The proof is detailed in Appendix A.3. □

Corollary 4. *Let $\epsilon > 0$ be given. Suppose that $\{a_n\}_{n=1}^{\infty}$ be a positive real sequence such that only finitely many elements are lower than $1 + \epsilon$. Then for any $x \in \mathbb{R} \setminus \{0\}$*

$$\lim_{m \to \infty} |\Phi_m(x)| \geq \xi_{1+\epsilon}.$$

Proof. The proof is detailed in Appendix A.4. □

Based on Proposition 3 and Corollary 4, if there exists a sufficiently large $N \in \mathbb{N}$ such that $a_n < 1$ (resp. $a_n > 1 + \epsilon$) for all $n \geq N$, then for any $x_0 \in \mathbb{R} \setminus \{0\}$, $\Phi_m(x_0) \to 0$ (resp. $|\Phi_m(x_0)| \geq \xi_{1+\epsilon}$) as $m \to \infty$. This result implies that if the sequence $\{\Phi_m\}_{m=1}^{M}$ is finite, a_n for $N \leq n \leq M$, where N is an arbitrarily chosen index close to M, significantly influence the values of $\Phi_M(x_0)$.

3.2 The derivation of the proposed weight initialization method

Based on the theoretical motivations discussed in the previous section, we propose a weight initialization method that satisfies the following conditions during the initial forward pass:

(i) It prevents activation values from vanishing towards zero in deep layers.

(ii) It ensures that the distribution of activation values in deep layers is approximately normal.

Notations. Consider a feedforward neural network with L layers. The network processes K training samples, denoted as pairs $\{(\boldsymbol{x}_i, \boldsymbol{y}_i)\}_{i=1}^{K}$, where $\boldsymbol{x}_i \in \mathbb{R}^{N_x}$ is training input and $\boldsymbol{y}_i \in \mathbb{R}^{N_y}$ is its corresponding output. The iterative computation at each layer ℓ is defined as follows:

$$\boldsymbol{x}^{\ell} = \tanh(\mathbf{W}^{\ell}\boldsymbol{x}^{\ell-1} + \mathbf{b}^{\ell}) \in \mathbb{R}^{N_\ell} \quad \text{for all } \ell = 1, \ldots, L,$$

where $\mathbf{W}^{\ell} \in \mathbb{R}^{N_\ell \times N_{\ell-1}}$ is the weight matrix, $\mathbf{b}^{\ell} \in \mathbb{R}^{N_\ell}$ is the bias, and $\tanh(\cdot)$ is an element-wise activation hyperbolic tangent function. Denote $\mathbf{W}^{\ell} = [w_{ij}^{\ell}]$.

Signal Propagation Analysis. We present a simplified analysis of signal propagation in FFNNs with the tanh activation function. For notational convenience, it is assumed that all hidden layers, as well

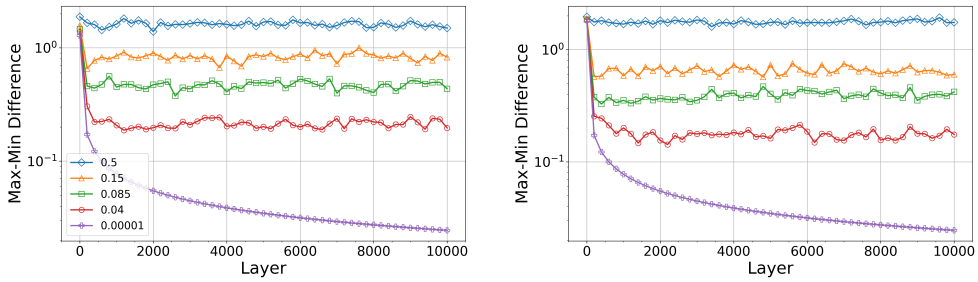

(a) Same dimension

(b) Varying dimensions

Figure 2: Difference between the maximum and minimum activation values at each layer when propagating $3,000$ input samples through a $10,000$-layer tanh FFNN, using the proposed initialization with α set to $0.04, 0.085, 0.15$, and 0.5. Network with $10,000$ hidden layers, each with 32 nodes **(left)**, and a network with alternating hidden layers of 64 and 32 nodes **(right)**.

as the input and output layers, have a dimension of n, i.e., $N_\ell = n$ for all ℓ. Given an arbitrary input vector $\boldsymbol{x} = (x_1, \ldots, x_n)$, the first layer activation $\boldsymbol{x}^1 = \tanh(\mathbf{W}^1\boldsymbol{x})$ can be expressed component-wise as

$$x_i^1 = \tanh\left(w_{i1}^1 x_1 + \cdots + w_{in}^1 x_n\right) = \tanh\left(\left(w_{ii}^1 + \sum_{\substack{j=1\\ j\neq i}}^{n} \frac{w_{ij}^1 x_j}{x_i}\right) x_i\right) \text{ for } i = 1, \ldots, n.$$

For the $(k+1)$-th layer this expression can be generalized as

$$x_i^{k+1} = \tanh\left(a_i^{k+1} x_i^k\right), \text{ where } \quad a_i^{k+1} = w_{ii}^{k+1} + \sum_{\substack{j=1\\ j\neq i}}^{n} \frac{w_{ij}^{k+1} x_j^k}{x_i^k} \quad \text{for } i = 1, \ldots, n. \tag{1}$$

Equation (1) follows the form of $\tanh(ax)$, as discussed in Section 3.2. According to Lemma 2, when $a > 1$, for an arbitrary initial value $x_0 > 0$ or $x_0 < 0$, the sequence $\{x_k\}$ defined by $x_{k+1} = \tanh(ax_k)$ converges to ξ_a or $-\xi_a$, respectively, as $k \to \infty$. This result indicates that the sequence converges to the fixed point ξ_a regardless of the initial value x_0. From the perspective of signal propagation in tanh-based FFNNs, this ensures that the activation values do not vanish as the network depth increases. Furthermore, by Proposition 3, if $a_i^k \leq 1$ for all $N \leq k \leq L$, where N is an arbitrarily chosen index close to L, the value of x_i^L approaches zero. Therefore, to satisfy condition (i), a_i^k remains close to 1, and the inequality $a_i^k \leq 1$ does not hold for all $N \leq k \leq L$.

Proposed Weight Initialization. The proposed initial weight matrix is defined as $\mathbf{W}^\ell = \mathbf{D}^\ell + \mathbf{Z}^\ell \in \mathbb{R}^{N_\ell \times N_{\ell-1}}$, where $\mathbf{D}_{i,j}^\ell = 1$ if $i \equiv j \pmod{N_{\ell-1}}$, 0 otherwise (Examples of $\mathbf{D}^\ell$ are provided in Appendix D). The noise matrix $\mathbf{Z}^\ell$ is drawn from $\mathcal{N}(0, \sigma_z^2)$, where σ_z is set to $\alpha/\sqrt{N^{\ell-1}}$ with $\alpha = 0.085$. Then a_i^{k+1} follows the distribution:

$$a_i^{k+1} \sim \mathcal{N}\left(1,\, \sigma_z^2 + \sigma_z^2 \sum_{\substack{j=1\\ j\neq i}}^{n} \left(\frac{x_j^k}{x_i^k}\right)^2\right). \tag{2}$$

According to Equation (2), a_i^{k+1} follows a Gaussian distribution with a mean of 1. Additionally, if x_i^k becomes small relative to other elements in $\boldsymbol{x}^k$, the variance of the distribution in (2) increases. Consequently, the probability that the absolute value of x_i^{k+1} exceeds that of x_i^k becomes higher. Figure 1 (b) shows that activation values maintain consistent scales in deeper layers.

3.3 Preventing activation saturation via appropriate σ_z tuning

In this section, we determine the appropriate value of α in $\sigma_z = \alpha/\sqrt{N_{\ell-1}}$ that satisfies condition (ii). Condition (ii) is motivated by normalization methods (Ioffe, 2015; Ba, 2016). Firstly,

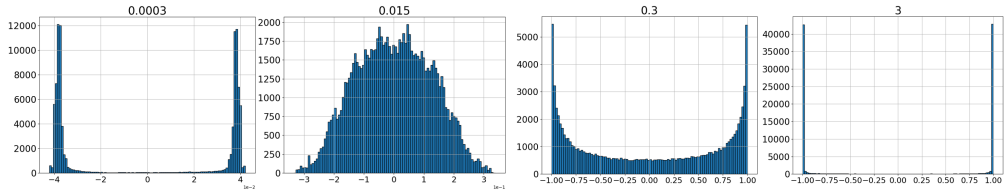

Figure 3: The activation values in the 1000th layer, with 32 nodes per hidden layer, were analyzed using the proposed weight initialization method with σ_z values of 0.0003, 0.015, 0.3, and 3. The analysis was conducted on 3000 input samples uniformly distributed within the range $[-1, 1]$.

we experimentally investigated the impact of σ_z on the scale of the activation values. As shown in Figure 2, increasing $\sigma_z = \alpha/\sqrt{N_{\ell-1}}$ broadens the activation range in each layer, while decreasing σ_z narrows it.

When σ_z is Large. Setting σ_z to a large value can lead to saturation. If σ_z is too large, Equation (2) implies that the likelihood of a_i^k deviating significantly from 1 increases. This increases the likelihood of activation values being bounded by $\xi_{1+\epsilon}$ in sufficiently deep layers, as stated in Corollary 4. Consequently, in deeper layers, activation values are less likely to approach zero and tend to saturate toward specific values. Please refer to the Figure 3 for the cases where $\sigma_z = 0.3$ and 3.

When σ_z is Small. If σ_z is too small, Equation (2) implies that the distribution of a_i^k has a standard deviation close to zero. Consequently, x_i^{k+1} can be approximated as the result of applying $\tanh(x)$ to $x_i > 0$ repeatedly for a finite number of iterations, k. Since $\tanh'(x)$ decreases for $x \geq 0$, the values resulting from finite iterations eventually saturate. Plese refer to the Figure 3 when $\sigma_z = 0.0003$.

For these reasons, we experimentally determined an optimal σ_z that avoids being excessively large or small. As shown in Figure 3, $\sigma_z = 0.015$ maintains an approximately normal activation distribution without collapse. Additional experimental results are provided in Appendix B.1. Considering the number of hidden layer nodes, we set $\sigma_z = \alpha/\sqrt{N^{\ell-1}}$ with $\alpha = 0.085$. Experimental results for solving the Burgers' equation using PINNs with varying σ_z are provided in Appendix C.3.

4 Experiments

In this section, we present a series of experiments to evaluate the proposed weight initialization method. In Section 4.1, we evaluate the performance of tanh FFNNs on benchmark datasets. In Section 4.2, we apply Physics-Informed Neural Networks to solve PDEs. Both experiments assess the proposed method's robustness to network size and data efficiency.

Table 1: Validation accuracy and loss are presented for FFNNs with varying numbers of nodes $(2, 8, 32, 128, 512)$, each with 20 hidden layers using tanh activation function. All models were trained for 20 epochs, and the highest average accuracy and lowest average loss, computed over 10 runs, are presented. The better-performing method is highlighted in bold when comparing different initialization methods under the same experimental settings.

Dataset	Method	2 Nodes		8 Nodes		32 Nodes		128 Nodes		512 Nodes	
		Accuracy	Loss	Accuracy	Loss	Accuracy	Loss	Accuracy	Loss	Accuracy	Loss
MNIST	Xavier	49.78	1.632	68	0.958	91.67	0.277	95.45	0.154	97.35	0.087
	Proposed	**62.82**	**1.185**	**77.95**	**0.706**	**92.51**	**0.255**	**96.12**	**0.134**	**97.96**	**0.067**
FMNIST	Xavier	42.89	1.559	68.55	0.890	81.03	0.533	86.20	0.389	88.28	0.331
	Proposed	**51.65**	**1.324**	**71.31**	**0.777**	**83.06**	**0.475**	**87.12**	**0.359**	**88.59**	**0.323**
CIFAR-10	Xavier	32.82	1.921	43.51	1.608	48.62	1.473	47.58	1.510	51.71	1.369
	Proposed	**38.16**	**1.780**	**47.04**	**1.505**	**48.80**	**1.463**	**48.51**	**1.471**	**52.21**	**1.359**
CIFAR-100	Xavier	10.87	4.065	18.53	3.619	23.71	3.301	23.83	3.324	17.72	3.672
	Proposed	**15.22**	**3.818**	**23.07**	**3.350**	**24.93**	**3.237**	**24.91**	**3.240**	**22.80**	**3.435**

Table 2: Validation accuracy and loss are presented for FFNNs with varying numbers of layers $(3, 10, 50, 100)$, each with 64 number of nodes using the tanh activation function. All models were trained for 40 epochs, and the highest average accuracy and lowest average loss, computed over 10 runs, are presented.

Dataset	Method	3 Layers		10 Layers		50 Layers		100 Layers	
		Accuracy	Loss	Accuracy	Loss	Accuracy	Loss	Accuracy	Loss
MNIST	Xavier	95.98	0.130	96.55	0.112	96.57	0.123	94.08	0.194
	Proposed	**96.32**	**0.123**	**97.04**	**0.102**	**96.72**	**0.109**	**96.06**	**0.132**
FMNIST	Xavier	85.91	0.401	88.73	0.319	87.72	0.344	83.41	0.463
	Proposed	**86.51**	**0.379**	**89.42**	**0.305**	**88.51**	**0.324**	**86.01**	**0.382**
CIFAR-10	Xavier	42.91	1.643	48.39	1.468	47.87	1.474	46.71	1.503
	Proposed	**45.05**	**1.588**	**48.41**	**1.458**	**48.71**	**1.461**	**48.96**	**1.437**
CIFAR-100	Xavier	19.10	3.628	22.73	3.400	24.27	3.283	20.32	3.515
	Proposed	**19.30**	**3.609**	**23.83**	**3.309**	**25.07**	**3.190**	**24.41**	**3.234**

4.1 Classification Task

Experimental Setting. To evaluate the effectiveness of the proposed weight initialization method, we conduct experiments on the MNIST, Fashion MNIST (FMNIST), CIFAR-10, and CIFAR-100 (Krizhevsky & Hinton, 2009) datasets with the Adam optimizer. All experiments are performed with a batch size of 64 and a learning rate of 0.0001. Fifteen percent of the dataset is allocated for validation. The experiments are implemented in TensorFlow without skip connections and learning rate decay in any of the experiments.

Width Independence in Classification Task. We evaluate the proposed weight initialization method in training tanh FFNNs, focusing on its robustness across different network widths. Five tanh FFNNs are designed, each with 20 hidden layers, and with $2, 8, 32$, 128, and 512 nodes per hidden layer, respectively. In Table 1, for the MNIST, Fashion MNIST and CIFAR-10 datasets, the network with 512 nodes achieves the highest accuracy and lowest loss when the proposed method is employed. However, for the CIFAR-100 dataset, the network with 32 nodes yields the highest accuracy and lowest loss when employing the proposed method. In summary, the proposed method demonstrates robustness across different network widths in tanh FFNNs. Detailed experimental results are provided in Appendix B.2.

Depth Independence in Classification Task. The expressivity of neural networks is known to increase exponentially with depth, leading to improved generalization performance (Poole et al., 2016; Raghu et al., 2017). To evaluate the robustness of the proposed weight initialization method across different network depths, we conduct experiments on deep FFNNs with tanh activation functions. Specifically, we construct four tanh FFNNs, each with 64 nodes per hidden layer and 3, 10, 50, or 100 hidden layers. respectively. In Table 2, for both the MNIST and Fashion MNIST datasets, the network with 10 hidden layers achieves the highest accuracy and lowest loss when our proposed method is employed. Both initialization methods exhibit lower performance in networks with 3 layers compared to those with more layers. Moreover, for more complex datasets such as CIFAR-10 and CIFAR-100, the proposed method demonstrated improved performance when training deeper networks.

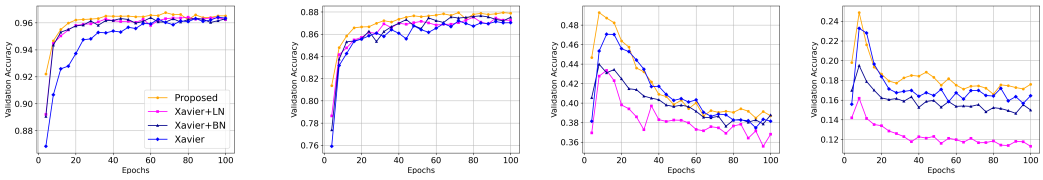

(a) MNIST (b) Fashion MNIST (c) CIFAR10 (d) CIFAR100

Figure 4: Validation accuracy for a tanh FFNN with 50 hidden layers (32 nodes each). Xavier + BN and Xavier + LN represent Xavier initialization with Batch Normalization or Layer Normalization applied every 5 layers, respectively.

Table 3: Validation accuracy and loss for a 10-layer FFNN (64 nodes per layer) trained on datasets containing 10, 20, 30, 50, and 100 samples. Results show the highest average accuracy and lowest average loss over 5 runs after 100 epochs.

Dataset	Method	10		20		30		50		100	
		Accuracy	Loss	Accuracy	Loss	Accuracy	Loss	Accuracy	Loss	Accuracy	Loss
MNIST	Xavier	31.13	2.281	35.03	2.078	45.05	1.771	58.45	1.227	64.02	1.139
	Xavier + BN	22.46	2.267	33.73	2.053	37.13	2.042	39.78	1.944	57.51	1.464
	Xavier + LN	28.52	2.411	41.54	1.796	41.94	1.886	54.97	1.362	65.11	1.093
	Proposed	**37.32**	**2.204**	**46.79**	**1.656**	**48.60**	**1.645**	**61.54**	**1.131**	**68.44**	**1.043**
FMNIST	Xavier	36.16	2.320	41.69	1.814	53.86	1.459	64.53	1.140	63.58	1.048
	Xavier + BN	35.44	**2.136**	38.58	1.925	40.16	1.819	53.93	1.728	59.78	1.237
	Xavier + LN	34.94	2.362	37.90	1.793	53.27	1.470	59.50	1.198	62.01	1.073
	Proposed	**37.31**	2.217	**49.25**	**1.651**	**55.19**	**1.372**	**66.14**	**1.057**	**67.58**	**0.914**

Normalization Methods. Xavier initialization is known to cause vanishing gradients and activation problems in deeper networks. These issues can be mitigated by applying Batch Normalization (BN) or Layer Normalization (LN) in the network. Therefore, we compare the proposed method with Xavier, Xavier with BN, and Xavier with LN. To evaluate the effectiveness of normalization, we conducted experiments using a sufficiently deep neural network with 50 hidden layers. As shown in Figure 4, for datasets with relatively fewer features, such as MNIST and FMNIST, Xavier with normalization converges faster than Xavier. However, for feature-rich datasets such as CIFAR-10 and CIFAR-100, the accuracy of Xavier with normalization is lower than that of Xavier. Normalization typically incurs a 30% computational overhead, and additional hyperparameter tuning is required to determine which layers should apply normalization. In contrast, the proposed method achieves the best performance across all datasets without requiring normalization.

Data Efficiency in Classification Task. Based on the results in Table 2, we evaluated data efficiency on a network with 50 hidden layers, each containing 64 nodes, where Xavier exhibited strong performance. As shown in Table 3, the highest average accuracy and lowest average loss over 5 runs after 100 epochs are presented for datasets containing 10, 20, 30, 50, and 100 samples. The proposed method achieved the best performance across all sample sizes.

Non-uniform Hidden Layer Dimensions. We evaluate the performance of the proposed initialization in networks where hidden layer dimensions are not uniform. As shown in Figure 5, the network consists of 60 hidden layers, where the number of nodes alternates between 32 and 16 in each layer. The proposed method demonstrates improved performance in terms of both loss and accuracy across all epochs on the MNIST and CIFAR-10 datasets. Additionally, Appendix B.3 presents experiments on networks with larger variations in the number of nodes. Motivated by these results, Appendix B.3 further explores autoencoders with significant differences in hidden layer dimensions.

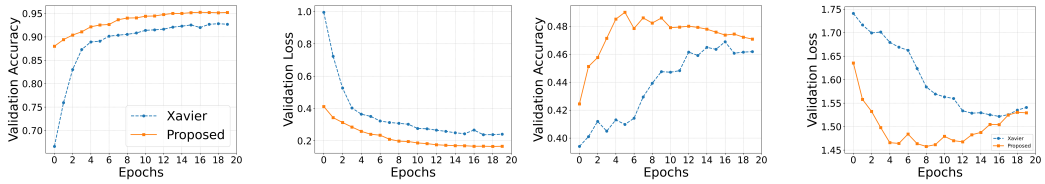

(a) MNIST Accuracy (b) MNIST Loss (c) CIFAR10 Accuracy (d) CIFAR10 Loss

Figure 5: Validation accuracy and loss for a tanh FFNN with 60 hidden layers, where the number of nodes alternates between 32 and 16 across layers, repeated 30 times. The model was trained for 20 epochs on the MNIST and CIFAR-10 datasets.

4.2 Physics-Informed Neural Networks

Xavier initialization is the most commonly employed method for training PINNs (Jin et al., 2021; Son et al., 2023; Yao et al., 2023; Gnanasambandam et al., 2023). In this section, we experimentally demonstrate that the proposed method is more robust across different network sizes and achieves better data efficiency compared to Xavier initialization with or without normalization methods.

Experimental Setting. All experiments on Physics-Informed Neural Networks (PINNs) use full-batch training with a learning rate of 0.001. In this section, we solve the Allen-Cahn, Burgers, Diffusion, and Poisson equations using a tanh FFNN-based PINN with 20,000 collocation points. Details on the PDEs are provided in Appendix C.1.

Network Size Independence in PINNs. We construct eight tanh FFNNs, each with 16 nodes per hidden layer and $5, 10, 20, 30, 40, 50, 60,$ or 80 hidden layers. As shown in Table 4, for the Allen-Cahn and Burgers' equations, Xavier+BN and Xavier+LN achieve the lowest loss at a network depth of 30. However, their loss gradually increases as depth grows. In contrast, the proposed method achieves the lowest loss at depths of 50 and 60, respectively, maintaining strong learning performance even in deeper networks. For the Diffusion and Poisson equations, Xavier+LN achieves the lowest loss at depths of 5 and 10, respectively. While all methods exhibit increasing loss as network depth increases, the proposed method consistently maintains lower loss in deeper networks. Similar trends are observed with 32 nodes. Across all tested network sizes and PDEs, the proposed method consistently achieves the lowest loss. The proposed method eliminates the computational overhead and hyperparameter tuning required for normalization methods.

Table 4: A PINN loss is presented for FFNNs with varying numbers of layers $(5, 10, 20, 30, 40, 50, 60, 80)$ using the tanh activation function. The top table shows results with 16 nodes per layer, and the bottom table shows results with 32 nodes per layer. All models were trained for 300 iterations using Adam and 300 iterations using L-BFGS. The median PINN loss from the final iteration for the Burgers, Allen–Cahn, Diffusion, and Poisson equations, computed over 5 runs, is presented.

Allen-Cahn (16 Nodes)	5	10	20	30	40	50	60	80
Xavier	9.58e-04	8.16e-04	7.61e-04	1.06e-03	1.1e-03	1.24e-03	3.55e-03	1.81e-03
Xavier + BN	1.42e-03	8.17e-04	8.56e-04	7.07e-04	7.77e-04	8.87e-04	9.11e-04	2.15e-03
Xavier + LN	6.29e-01	1.77e-03	6.98e-04	1.27e-03	1.82e-03	6.65e-01	3.29e-01	5.86e-01
Proposed	**9.21e-04**	**7.29e-04**	**5.76e-04**	**5.29e-04**	**5.37e-04**	**4.03e-04**	**4.73e-04**	**5.77e-04**
Burgers (16 Nodes)	5	10	20	30	40	50	60	80
Xavier	6.97e-03	1.11e-02	7.9e-03	9.71e-03	2.45e-02	2.65e-02	6.5e-02	5.71e-02
Xavier + BN	8.07e-03	7.72e-03	6.24e-03	1.70e-02	1.50e-02	1.85e-02	2.91e-02	6.84e-02
Xavier + LN	3.89e-02	1.88e-02	9.48e-03	9.28e-03	2.46e-02	3.30e-02	6.91e-02	4.42e-02
Proposed	**6.19e-03**	**5.08e-03**	**5.28e-03**	**9.31e-04**	**3.56e-03**	**8.27e-04**	**3.43e-04**	**2.05e-03**
Diffusion (16 Nodes)	5	10	20	30	40	50	60	80
Xavier	2.52e-03	4.82e-03	9.69e-03	1.33e-02	2.08e-02	1.50e-02	2.92e-02	7.24e-02
Xavier + BN	2.89e-03	5.77e-03	1.05e-02	9.65e-03	2.76e-02	1.07e-02	9.07e-03	1.43e-02
Xavier + LN	1.72e-03	6.10e-03	8.04e-03	9.48e-03	2.14e-02	7.59e-03	2.05e-02	2.21e-02
Proposed	**9.14e-04**	**2.59e-03**	**2.40e-03**	**1.01e-03**	**1.97e-03**	**1.21e-03**	**1.12e-03**	**1.91e-03**
Poisson (16 Nodes)	5	10	20	30	40	50	60	80
Xavier	1.52e-02	2.87e-02	1.28e-01	9.82e-02	1.15e-01	1.37e-01	1.82e-01	2.55e-01
Xavier + BN	1.62e-02	2.02e-02	8.72e-02	1.12e-01	2.45e-01	9.85e-02	1.00e-01	1.34e-01
Xavier + LN	5.39e-01	4.40e-02	1.34e-01	3.91	2.52e+02	2.58	9.79e+02	nan
Proposed	**1.37e-02**	**1.70e-02**	**4.62e-02**	**2.43e-02**	**3.75e-02**	**4.03e-02**	**6.07e-02**	**6.01e-02**

Allen-Cahn (32 Nodes)	5	10	20	30	40	50	60	80
Xavier	3.13e-01	5.03e-02	3.64e-03	2.37e-03	4.03e-03	5.27e-03	1.73e-02	6.94e-01
Xavier + BN	4.05e-01	8.85e-04	8.41e-04	7.82e-04	9.97e-04	6.80e-04	9.34e-04	6.94e-01
Xavier + LN	3.31e-01	2.10e-03	5.99e-04	6.71e-04	1.49e-03	1.29e-03	3.31e-02	6.93e-01
Proposed	**1.04e-03**	**6.92e-04**	**5.34e-04**	**4.26e-04**	**3.31e-04**	**3.52e-04**	**3.85e-04**	**5.96e-04**
Burgers (32 Nodes)	5	10	20	30	40	50	60	80
Xavier	1.12e-02	3.53e-03	2.72e-03	1.81e-03	7.60e-03	8.56e-03	9.86e-03	1.66e-01
Xavier + BN	5.88e-03	**1.04e-03**	1.79e-03	2.80e-03	5.95e-03	3.66e-02	6.60e-02	1.66e-01
Xavier + LN	4.31e-02	1.21e-02	1.88e-03	7.22e-03	5.54e-03	8.46e-03	9.04e-03	4.86e-02
Proposed	**4.14e-03**	4.11e-03	**1.58e-03**	**1.29e-03**	**7.96e-04**	**5.85e-04**	**9.80e-04**	**1.47e-03**
Diffusion (32 Nodes)	5	10	20	30	40	50	60	80
Xavier	1.69e-03	6.85e-03	7.63e-03	4.50e-03	8.98e-03	5.67e-03	6.33e-01	1.59
Xavier + BN	1.68e-03	2.66e-03	1.08e-02	6.00e-03	8.58e-03	6.60e-03	5.66e-02	1.69e+02
Xavier + LN	8.16e-04	2.85e-03	8.46e-03	4.57e-03	9.40e-03	1.04e-02	2.42e-01	1.67e+02
Proposed	**2.89e-04**	**8.03e-04**	**5.25e-04**	**5.07e-04**	**5.33e-04**	**6.17e-04**	**9.80e-04**	**1.53e-03**
Poisson (32 Nodes)	5	10	20	30	40	50	60	80
Xavier	1.09e-02	1.33e-02	3.13e-02	7.69e-02	6.72e-02	8.90e-02	9.68e+02	1.46e+02
Xavier + BN	1.14e-02	1.47e-02	2.68e-02	3.55e-02	8.25e-02	8.97e-02	4.50e-02	7.75e-01
Xavier + LN	2.36e-02	2.18e-02	3.07e-02	3.85e-01	1.40	4.69	2.60	6.14
Proposed	**9.63e-03**	**8.29e-03**	**1.41e-02**	**1.88e-02**	**1.65e-02**	**1.85e-02**	**1.73e-02**	**3.59e-02**

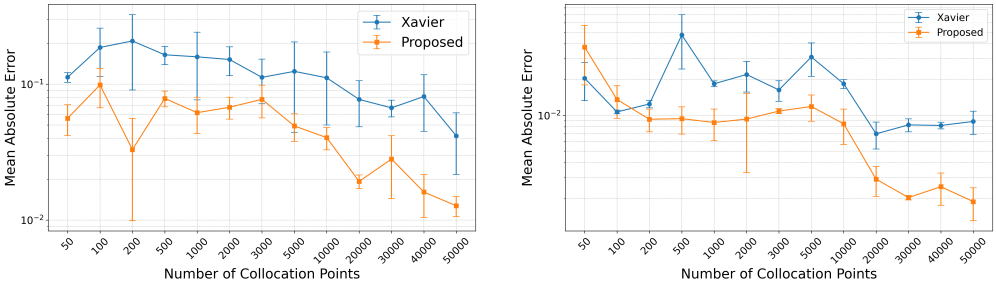

(a) Burgers Equation

(b) Diffusion Equation

Figure 6: Mean absolute error between the exact solution and PINN-predicted solution with varying numbers of collocation points. The FFNN has 30 hidden layers (32 nodes each) and is trained for 300 iterations using Adam followed by 300 iterations using L-BFGS. The results are averaged over 5 experiments.

Data Efficiency in PINNs. Based on the results in Table 4, we evaluate data efficiency on a network with 30 hidden layers, each containing 32 nodes, where Xavier initialization achieved the lowest PINN loss. As shown in Figure 6, for the Burgers equation, the Mean Absolute Error (MAE) of the proposed initialization differs significantly from that of Xavier initialization across varying numbers of collocation points. In contrast, for the Diffusion equation, the difference in MAE between the two methods becomes more pronounced when the number of collocation points exceeds $20,000$. Additionally, Figure 7 illustrates that increasing the number of collocation points enables PINNs with the proposed initialization to predict solutions with lower absolute error. For detailed experiments on the Burgers equation, please refer to Appendix C.4.

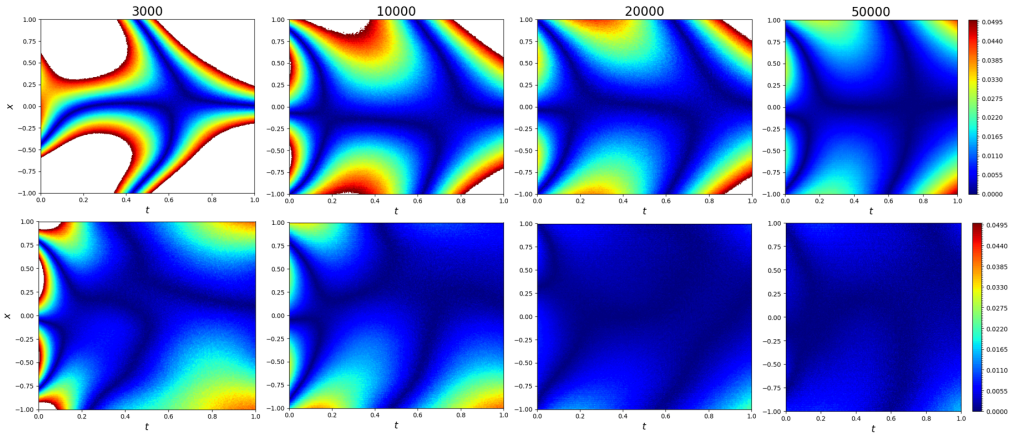

Figure 7: Absolute error between the exact solution and the PINN-predicted solution for the Diffusion equation with varying numbers of collocation points $(3000, 10000, 20000, 50000)$ using **(upper row)** Xavier and **(lower row)** the proposed initialization. The FFNN has 30 hidden layers (32 nodes each) and is trained for 300 iterations using Adam followed by 300 iterations using L-BFGS. The color bar ranges from 0 to 0.05, with values outside this range shown in white.

5 Conclusion

In this study, we proposed a novel weight initialization method for tanh neural networks, grounded in the theoretical analysis of fixed points of the $\tanh(ax)$ function. The proposed method is experimentally demonstrated to achieve robustness to variations in network size without normalization methods and to exhibit improved data efficiency. Therefore, the proposed weight initialization method reduces the time and effort required for training on large datasets and optimizing network architectures.

ACKNOWLEDGMENTS

This work of Hyunwoo Lee and Hayoung Choi was supported by the National Research Foundation of Korea(NRF) grant funded by the Korea government(MSIT) (No. 2022R1A5A1033624 and RS-2024-00342939). The work of Hyunju Kim was supported by the funds of the Open R&D program of Korea Electric Power Corporation.(No-R23XO03).

REFERENCES

Jimmy Lei Ba. Layer normalization. *arXiv preprint arXiv:1607.06450*, 2016.

Thomas Bachlechner, Bodhisattwa Prasad Majumder, Henry Mao, Gary Cottrell, and Julian McAuley. Rezero is all you need: Fast convergence at large depth. In *Uncertainty in Artificial Intelligence*, pp. 1352–1361. PMLR, 2021.

Hassan Bararnia and Mehdi Esmaeilpour. On the application of physics informed neural networks to solve boundary layer thermal-fluid problems. *International Communications in Heat and Mass Transfer*, 132:105890, 2022.

Yoshua Bengio, Paolo Frasconi, and Patrice Simard. The problem of learning long-term dependencies in recurrent networks. In *IEEE International Conference on Neural Networks*, pp. 1183–1188. IEEE, 1993.

Djork-Arné Clevert. Fast and accurate deep network learning by exponential linear units (ELUs). *arXiv preprint arXiv:1511.07289*, 2015.

Salvatore Cuomo, Vincenzo Schiano Di Cola, Fabio Giampaolo, Gianluigi Rozza, Maziar Raissi, and Francesco Piccialli. Scientific machine learning through physics–informed neural networks: Where we are and What's next. *Journal of Scientific Computing*, 92(3):88, 2022.

G. Cybenko. Approximation by superpositions of a sigmoidal function. *Mathematics of Control, Signals and Systems*, 2(4):303–314, 1989.

Xavier Glorot and Yoshua Bengio. Understanding the difficulty of training deep feedforward neural networks. In *International Conference on Artificial Intelligence and Statistics*, pp. 249–256, 2010.

Raghav Gnanasambandam, Bo Shen, Jihoon Chung, Xubo Yue, and Zhenyu Kong. Self-scalable tanh (stan): Multi-scale solutions for physics-informed neural networks. *IEEE Transactions on Pattern Analysis and Machine Intelligence*, 45(12):15588–15603, 2023.

G. Gripenberg. Approximation by neural networks with a bounded number of nodes at each level. *Journal of Approximation Theory*, 122(2):260–266, 2003.

Namig J. Guliyev and Vugar E. Ismailov. Approximation capability of two hidden layer feedforward neural networks with fixed weights. *Neurocomputing*, 316:262–269, 2018a.

Namig J. Guliyev and Vugar E. Ismailov. On the approximation by single hidden layer feedforward neural networks with fixed weights. *Neural Networks*, 98:296–304, 2018b.

John M. Hanna, José V. Aguado, Sebastien Comas-Cardona, Ramzi Askri, and Domenico Borzacchiello. Residual-based adaptivity for two-phase flow simulation in porous media using physics-informed neural networks. *Computer Methods in Applied Mechanics and Engineering*, 396: 115100, 2022.

Kaiming He, Xiangyu Zhang, Shaoqing Ren, and Jian Sun. Delving deep into rectifiers: Surpassing human-level performance on imagenet classification. In *Proceedings of the IEEE International Conference on Computer Vision*, pp. 1026–1034, 2015.

Kaiming He, Xiangyu Zhang, Shaoqing Ren, and Jian Sun. Deep residual learning for image recognition. In *Proceedings of the IEEE Conference on Computer Vision and Pattern Recognition*, pp. 770–778, 2016.

Kurt Hornik. Approximation capabilities of multilayer feedforward networks. *Neural Networks*, 4 (2):251–257, 1991.

Kurt Hornik, Maxwell Stinchcombe, and Halbert White. Multilayer feedforward networks are universal approximators. *Neural Networks*, 2(5):359–366, 1989.

Vahid Reza Hosseini, Abbasali Abouei Mehrizi, Afsin Gungor, and Hamid Hassanzadeh Afrouzi. Application of a physics-informed neural network to solve the steady-state bratu equation arising from solid biofuel combustion theory. *Fuel*, 332:125908, 2023.

Sergey Ioffe. Batch normalization: Accelerating deep network training by reducing internal covariate shift. *arXiv preprint arXiv:1502.03167*, 2015.

Ameya D Jagtap and George Em Karniadakis. Extended physics-informed neural networks (XPINNs): A generalized space-time domain decomposition based deep learning framework for nonlinear partial differential equations. *Communications in Computational Physics*, 28(5), 2020.

Ameya D Jagtap, Ehsan Kharazmi, and George Em Karniadakis. Conservative physics-informed neural networks on discrete domains for conservation laws: Applications to forward and inverse problems. *Computer Methods in Applied Mechanics and Engineering*, 365:113028, 2020.

Ameya D Jagtap, Zhiping Mao, Nikolaus Adams, and George Em Karniadakis. Physics-informed neural networks for inverse problems in supersonic flows. *Journal of Computational Physics*, 466:111402, 2022.

Xiaowei Jin, Shengze Cai, Hui Li, and George Em Karniadakis. Nsfnets (navier-stokes flow nets): Physics-informed neural networks for the incompressible navier-stokes equations. *Journal of Computational Physics*, 426:109951, 2021.

George Em Karniadakis, Ioannis G Kevrekidis, Lu Lu, Paris Perdikaris, Sifan Wang, and Liu Yang. Physics-informed machine learning. *Nature Reviews Physics*, 3(6):422–440, 2021.

Diederik P Kingma and Jimmy Ba. Adam: A method for stochastic optimization. *arXiv preprint arXiv:1412.6980*, 2014.

Alex Krizhevsky and Geoffrey Hinton. Learning multiple layers of features from tiny images. *Technical Report, Citeseer*, 2009.

Yann LeCun, Yoshua Bengio, and Geoffrey Hinton. Deep learning. *Nature*, 521(7553):436–444, 2015.

Hyunwoo Lee, Yunho Kim, Seung Yeop Yang, and Hayoung Choi. Improved weight initialization for deep and narrow feedforward neural network. *Neural Networks*, 176:106362, 2024.

Dong C Liu and Jorge Nocedal. On the limited memory bfgs method for large scale optimization. *Mathematical Programming*, 45(1):503–528, 1989.

Xu Liu, Xiaoya Zhang, Wei Peng, Weien Zhou, and Wen Yao. A novel meta-learning initialization method for physics-informed neural networks. *Neural Computing and Applications*, 34(17): 14511–14534, 2022.

Lu Lu, Yeonjong Shin, Yanhui Su, and George Em Karniadakis. Dying relu and initialization: Theory and numerical examples. *arXiv preprint arXiv:1903.06733*, 2019.

Lu Lu, Pengzhan Jin, Guofei Pang, Zhongqiang Zhang, and George Em Karniadakis. Learning nonlinear operators via deeponet based on the universal approximation theorem of operators. *Nature Machine Intelligence*, 2021.

Vitaly Maiorov and Allan Pinkus. Lower bounds for approximation by mlp neural networks. *Neurocomputing*, 25(1):81–91, 1999.

Zhiping Mao, Ameya D. Jagtap, and George Em Karniadakis. Physics-informed neural networks for high-speed flows. *Computer Methods in Applied Mechanics and Engineering*, 360:112789, 2020.

Dmytro Mishkin and Jiri Matas. All you need is a good init. In *International Conference on Learning Representations*, 2016.

Sejun Park, Chulhee Yun, Jaeho Lee, and Jinwoo Shin. Minimum width for universal approximation. In *International Conference on Learning Representations*, 2021.

Pai Peng, Jiangong Pan, Hui Xu, and Xinlong Feng. RPINNs: Rectified-physics informed neural networks for solving stationary partial differential equations. *Computers & Fluids*, 245:105583, 2022.

Ben Poole, Subhaneil Lahiri, Maithra Raghu, Jascha Sohl-Dickstein, and Surya Ganguli. Exponential expressivity in deep neural networks through transient chaos. *Advances in neural information processing systems*, 29, 2016.

Maithra Raghu, Ben Poole, Jon Kleinberg, Surya Ganguli, and Jascha Sohl-Dickstein. On the expressive power of deep neural networks. In *International Conference on Machine Learning*, pp. 2847–2854, 2017.

Maziar Raissi, Paris Perdikaris, and George E Karniadakis. Physics-informed neural networks: A deep learning framework for solving forward and inverse problems involving nonlinear partial differential equations. *Journal of Computational physics*, 378:686–707, 2019.

Prajit Ramachandran, Barret Zoph, and Quoc V Le. Searching for activation functions. *arXiv preprint arXiv:1710.05941*, 2017.

Pratik Rathore, Weimu Lei, Zachary Frangella, Lu Lu, and Madeleine Udell. Challenges in training PINNs: A loss landscape perspective. In *International Conference on Machine Learning*, 2024.

David E Rumelhart, Geoffrey E Hinton, and Ronald J Williams. Learning representations by back-propagating errors. *Nature*, 323(6088):533–536, 1986.

Andrew M Saxe, James McClelland, and Surya Ganguli. Exact solutions to the nonlinear dynamics of learning in deep linear neural networks. In *International Conference on Learning Representations*, 2014.

Zuowei Shen, Haizhao Yang, and Shijun Zhang. Optimal approximation rate of relu networks in terms of width and depth. *Journal de Mathématiques Pures et Appliquées*, 157:101–135, 2022.

Khemraj Shukla, Patricio Clark Di Leoni, James Blackshire, Daniel Sparkman, and George Em Karniadakis. Physics-informed neural network for ultrasound nondestructive quantification of surface breaking cracks. *Journal of Nondestructive Evaluation*, 39:1–20, 2020.

Khemraj Shukla, Ameya D Jagtap, and George Em Karniadakis. Parallel physics-informed neural networks via domain decomposition. *Journal of Computational Physics*, 447:110683, 2021.

Hwijae Son, Sung Woong Cho, and Hyung Ju Hwang. Enhanced physics-informed neural networks with augmented lagrangian relaxation method (AL-PINNs). *Neurocomputing*, 548:126424, 2023.

Yanjie Song, He Wang, He Yang, Maria Luisa Taccari, and Xiaohui Chen. Loss-attentional physics-informed neural networks. *Journal of Computational Physics*, 501:112781, 2024.

Homayoon Tarbiyati and Behzad Nemati Saray. Weight initialization algorithm for physics-informed neural networks using finite differences. *Engineering with Computers*, pp. 1–17, 2023.

Zhiyong Wu, Huan Wang, Chang He, Bing J. Zhang, Tao Xu, and Qinglin Chen. The application of physics-informed machine learning in multiphysics modeling in chemical engineering. *Industrial & Engineering Chemistry Research*, 62, 2023.

Zixue Xiang, Wei Peng, Xu Liu, and Wen Yao. Self-adaptive loss balanced physics-informed neural networks. *Neurocomputing*, 496:11–34, 2022.

Liu Yang, Xuhui Meng, and George Em Karniadakis. B-PINNs: Bayesian physics-informed neural networks for forward and inverse pde problems with noisy data. *Journal of Computational Physics*, 425:109913, 2021.

Jiachen Yao, Chang Su, Zhongkai Hao, Songming Liu, Hang Su, and Jun Zhu. Multiadam: Parameter-wise scale-invariant optimizer for multiscale training of physics-informed neural networks. In *International Conference on Machine Learning*, pp. 39702–39721. PMLR, 2023.

Dmitry Yarotsky. Error bounds for approximations with deep relu networks. *Neural Networks*, 94: 103–114, 2017.

Minglang Yin, Xiaoning Zheng, Jay D Humphrey, and George Em Karniadakis. Non-invasive inference of thrombus material properties with physics-informed neural networks. *Computer Methods in Applied Mechanics and Engineering*, 375:113603, 2021.

Jeremy Yu, Lu Lu, Xuhui Meng, and George Em Karniadakis. Gradient-enhanced physics-informed neural networks for forward and inverse pde problems. *Computer Methods in Applied Mechanics and Engineering*, 393:114823, 2022.

Lei Yuan, Yi-Qing Ni, Xiang-Yun Deng, and Shuo Hao. A-PINN: Auxiliary physics informed neural networks for forward and inverse problems of nonlinear integro-differential equations. *Journal of Computational Physics*, 462:111260, 2022.

Jiawei Zhao, Florian Tobias Schaefer, and Anima Anandkumar. Zero initialization: Initializing neural networks with only zeros and ones. *Transactions on Machine Learning Research*, 2022. ISSN 2835-8856.

Jing'ang Zhu, Yiheng Xue, and Zishun Liu. A transfer learning enhanced physics-informed neural network for parameter identification in soft materials. *Applied Mathematics and Mechanics*, 45 (10):1685–1704, 2024.

A PROOFS OF THE THEORETICAL RESULTS

A.1 PROOF OF LEMMA 1

Proof. Define $g(x) = \tanh(ax) - x$. Since $g(x)$ is continuous, and $g(-M) > 0$, $g(M) < 0$ for a large real number M, the Intermediate Value Theorem guarantees the existence of a point x such that $g(x) = 0$.

First, consider the case $0 < a \leq 1$. Since $0 < a \leq 1$, the derivative $g'(x) = a \cdot \text{sech}^2(ax) - 1$ satisfies $-1 \leq g'(x) \leq a - 1 < 0$ for all x. Hence, $g(x)$ is strictly decreasing and therefore $g(x)$ has the unique root. At $x = 0$, $\phi(0) = \tanh(a \cdot 0) = 0$. Hence, $x = 0$ is the unique fixed point.

Let us consider the case $a > 1$. For $0 < x \ll 1$, $\tanh(ax) - x \approx (a-1)x$. Since $a > 1$, $\tanh(ax) - x > 0$. On the other hand, since $|\tanh(ax)| < 1$ for all x,

$$\lim_{x\to\infty}[-1 - x] \leq \lim_{x\to\infty}[\tanh(ax) - x] \leq \lim_{x\to\infty}[1 - x].$$

By the squeeze theorem, $\lim_{x\to\infty}[\tanh(ax) - x] = -\infty$. By the intermediate value theorem, therefore, there exists at least one $x > 0$ such that $\tanh(ax) = x$. To establish the uniqueness of the positive fixed point, we investigate the derivative $g'(x) = a\,\text{sech}^2(ax) - 1$. We find the critical points to be $x = \pm\frac{1}{a}\sec^{-1}(\frac{1}{\sqrt{a}})$. It is straightforward to see that $g'(x) > 0$ in $\left(-\frac{1}{a}\sec^{-1}(\frac{1}{\sqrt{a}}), \frac{1}{a}\sec^{-1}(\frac{1}{\sqrt{a}})\right)$ and $g'(x) < 0$ in $\mathbb{R}\backslash\left(-\frac{1}{a}\sec^{-1}(\frac{1}{\sqrt{a}}), \frac{1}{a}\sec^{-1}(\frac{1}{\sqrt{a}})\right)$. i.e. $g(x) = 0$ has exactly two fixed points. Because $g(x)$ is an odd function, if x^* is a solution, then $-x^*$ is also a solution. Thus, for $a > 1$, there exists a unique positive fixed point if $x > 0$ and a unique negative fixed point if $x < 0$. □

A.2 PROOF OF LEMMA 2

Proof. (1) Since $(\tanh(ax))' = a\,\text{sech}^2(ax) < 1$ for all $x > 0$, it holds that $x_{n+1} = \phi_a(x_n) < x_n$ for all $n \in \mathbb{N}$. Thus the sequence $\{x_n\}_{n=1}^{\infty}$ is decreasing. Since $x_n > 0$ for all $n \in \mathbb{N}$, by the monotone convergence theorem, it converges to the fixed point $x^* = 0$.
(2) Let $x_0 < \xi_a$. Since $\phi'(x)$ decreasing for $x \geq 0$, with $\phi'(0) > 1$ and ξ_a is the unique fixed point for $x > 0$, it holds that $x_n < x_{n+1} < \xi_a$ for all $n \in \mathbb{N}$. Thus, by the monotone convergence theorem, the sequence converges to the fixed point ξ_a. The proof is similar when $x_0 > \xi_a$. □

A.3 PROOF OF PROPOSITION 3

Proof. Set $N = \max\{n | a_n > 1\}$. Define the sequences $\{b_n\}_{n=1}^{\infty}$ and $\{c_n\}_{n=1}^{\infty}$ such that $b_n = c_n = a_n$ for $n \leq N$, with $b_n = 0$ and $c_n = 1$ for $n > N$. Suppose that $\{\hat{\Phi}_m\}_{m=1}^{\infty}$ and $\{\tilde{\Phi}_m\}_{m=1}^{\infty}$ are sequences of functions defined as for each $m \in \mathbb{N}$

$$\hat{\Phi}_m = \phi_{b_m} \circ \phi_{b_{m-1}} \circ \cdots \circ \phi_{b_1}, \quad \tilde{\Phi}_m = \phi_{c_m} \circ \phi_{c_{m-1}} \circ \cdots \circ \phi_{c_1}.$$

Then, the inequality $\hat{\Phi}_m \leq \Phi_m \leq \tilde{\Phi}_m$ holds for all m. By Lemma 1, for any $x \geq 0$, we have $\lim_{m\to\infty}\hat{\Phi}_m = 0$ and $\lim_{m\to\infty}\tilde{\Phi}_m = 0$. Therefore, the Squeeze Theorem guarantees that $\lim_{m\to\infty}\Phi_m(x) = 0$. □

A.4 PROOF OF COROLLARY 4

Proof. Set $N = \max\{n \mid a_n < 1 + \epsilon\}$. Define the sequence $\{b_n\}_{n=1}^{\infty}$ such that $b_n = a_n$ for $n \leq N$, and $b_n = 1 + \epsilon$ for $n > N$. The remainder of the proof is analogous to the proof of Proposition 3. □

B CLASSIFIACATION TASKS

B.1 ACTIVATION DISTRIBUTION FOR NORMALLY DISTRIBUTED INPUT DATA.

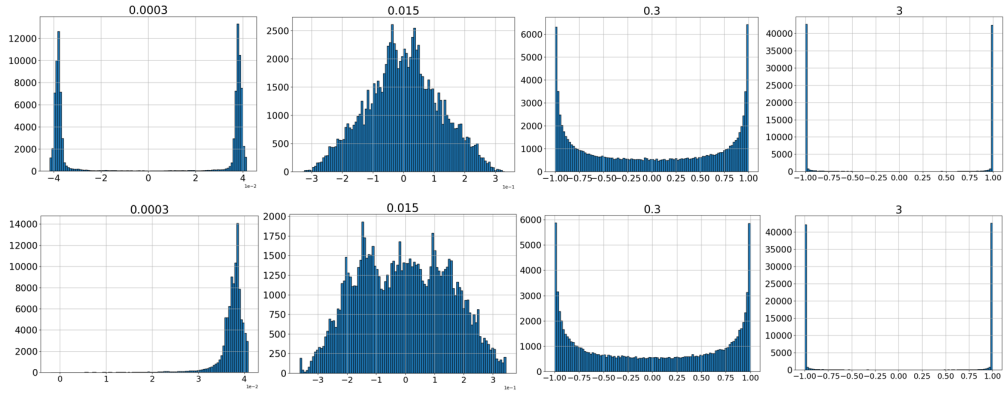

Figure 8: The activation values in the 1000th layer, with 32 nodes per hidden layer, were analyzed using the proposed weight initialization method with σ_z values of 0.0003, 0.015, 0.3, and 3. The **upper row** shows results for 3000 input samples drawn from a standard normal distribution, while the **lower row** presents results for samples drawn from a Beta distribution with parameters $a = 2.0$ and $b = 5.0$.

B.2 WIDTH INDEPENDENCE IN CLASSIFICATION TASKS

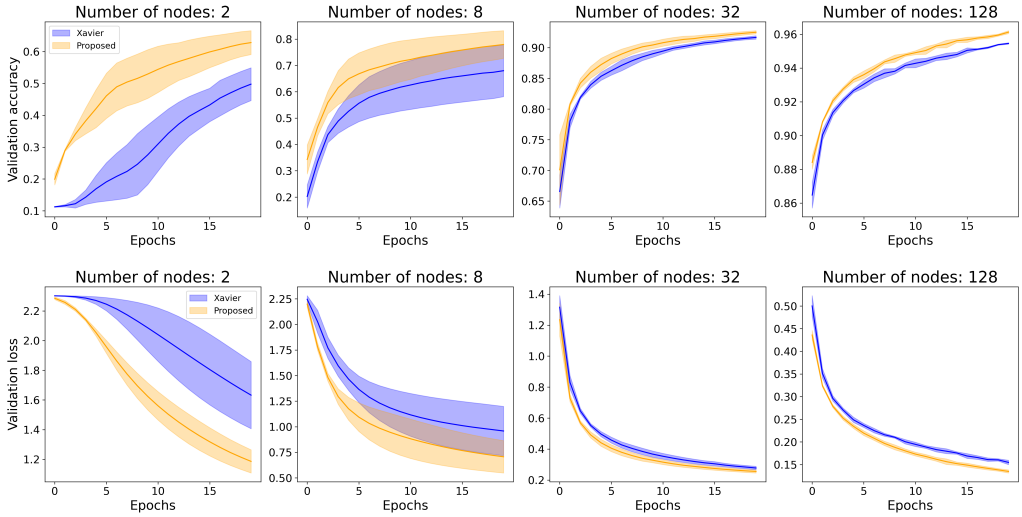

Figure 9: Validation accuracy and loss are presented for tanh FFNNs with varying numbers of nodes $(2, 8, 32, 128)$, each with 20 hidden layers. All models were trained for 20 epochs on the MNIST dataset, with 10 different random seeds.

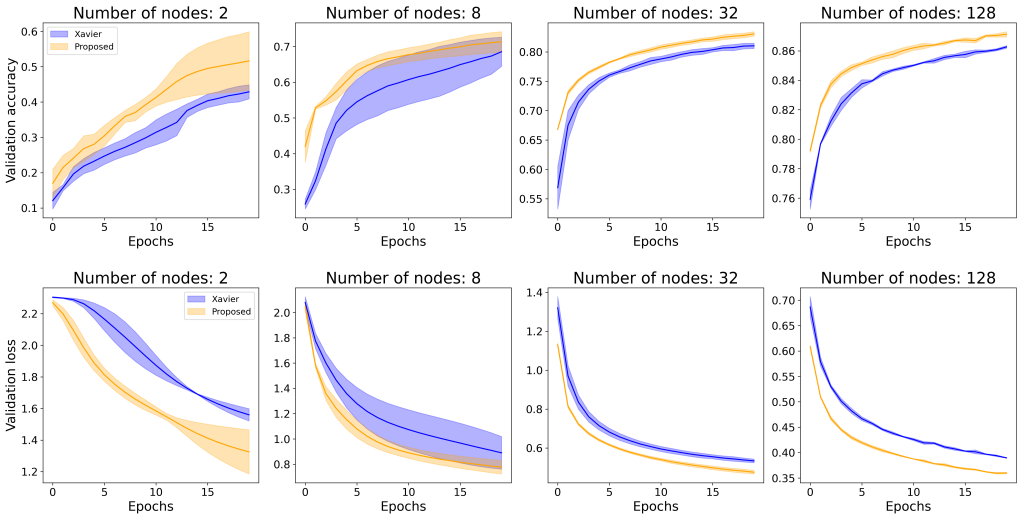

Figure 10: Validation accuracy and loss are presented for tanh FFNNs with varying numbers of nodes $(2, 8, 32, 128)$, each with 20 hidden layers. All models were trained for 20 epochs on the Fashion MNIST dataset, with 10 different random seeds.

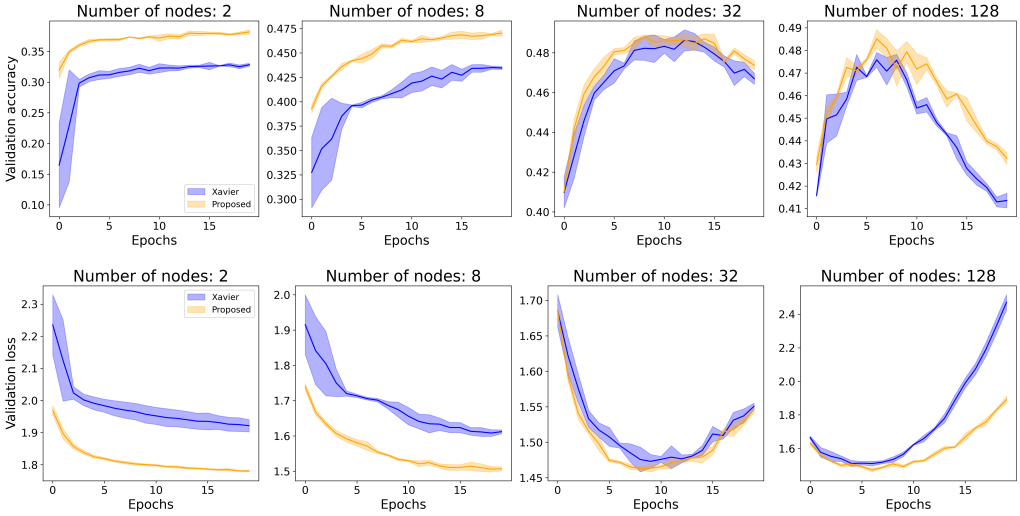

Figure 11: Validation accuracy and loss are presented for tanh FFNNs with varying numbers of nodes $(2, 8, 32, 128)$, each with 20 hidden layers. All models were trained for 20 epochs on the CIFAR-10 dataset, with 10 different random seeds.

B.3 Non-uniform Hidden Layer Dimensions

Tanh neural networks have been less commonly used compared to ReLU networks due to higher computational complexity, the vanishing gradient problem, and ReLU's superior empirical performance in many deep learning tasks. However, recent success of PINNs with tanh neural networks has led to a resurgence in their usage. In this section, we compare the performance of four methods on architectures that are generally challenging to train: (1) tanh activation with Xavier initialization, (2) tanh activation with the proposed initialization, (3) ReLU activation with He initialization + BN, and (4) ReLU activation with orthogonal initialization.

FFNN The experiments were conducted on an FFNN with alternating hidden layers of 16 and 4 nodes, repeated 50 times, over 100 epochs. The results are shown in Figure 13 (a). Both Xavier and

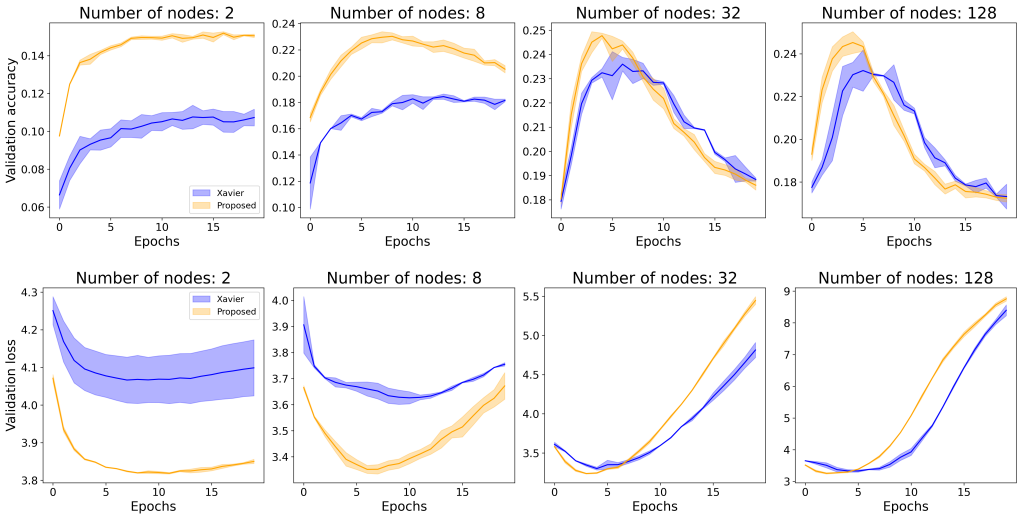

Figure 12: Validation accuracy and loss are presented for tanh FFNNs with varying numbers of nodes $(2, 8, 32, 128)$, each with 20 hidden layers. All models were trained for 20 epochs on the CIFAR-100 dataset, with 10 different random seeds.

the proposed method successfully trained the network, with the proposed method showing overall better performance. Given its strong performance despite significant differences in the number of nodes between hidden layers, we further tested the proposed method on autoencoders with large variations in layer sizes, as shown in Figure 13 (b).

Autoencoder The autoencoder architecture consists of an encoder and a decoder, both employing batch normalization and dropout (0.2) for regularization. The encoder compresses the input through layers of sizes 512, 256, 128, and finally maps to a latent space of 64 units. The decoder reconstructs the input by symmetrically expanding the latent space through layers of sizes 128, 256, and 512, followed by a final output layer with sigmoid activation. In Figure 13 (b), the model is trained on the MNIST dataset with a batch size of 256, while in (c), it is trained on the FMNIST dataset with a batch size of 512.

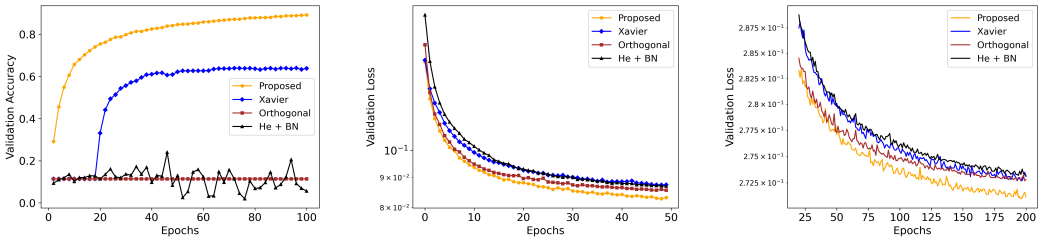

(a) FFNN (MNIST) (b) Autoencoder (MNIST) (c) Autoencoder (FMNIST)

Figure 13: **(a)** Validation loss for an FFNN with alternating hidden layers of 16 and 4 nodes, repeated 50 times, comparing four methods: Tanh with Xavier initialization, Tanh with the proposed initialization, ReLU with He initialization + BN, and ReLU with orthogonal initialization. **(b)** Validation loss for an autoencoder with encoder-decoder layers of 512, 256, 128, and 64 units, comparing the same four methods. **(c)** Same as (b), but on the FMNIST dataset.

C PHYSICS INFORMED NEURAL NETWORKS

C.1 PDE DETAILS

Allen-Cahn Equation The diffusion coefficient is set to $d = 0.01$. The initial condition is defined as $u(x, 0) = x^2 \cos(\pi x)$ for $x \in [-1, 1]$, with boundary conditions $u(-1, t) = -1$ and $u(1, t) = -1$, applied over the time interval $t \in [0, 1]$. The Allen-Cahn equation is expressed as

$$\frac{\partial u}{\partial t} - d\frac{\partial^2 u}{\partial x^2} = -\frac{u^3 + u}{d},$$

where $u(x, t)$ represents the solution, d is the diffusion coefficient, and the nonlinear term $u^3 - u$ models the phase separation dynamics.

Burgers' Equation The Burgers' equation, a viscosity coefficient of $\nu = 0.01$ is employed. The initial condition is given by $u(x, 0) = -\sin(\pi x)$ for $x \in [-1, 1]$, with boundary conditions $u(-1, t) = 0$ and $u(1, t) = 0$ imposed for $t \in [0, 1]$. The Burgers' equation is expressed as

$$\frac{\partial u}{\partial t} + u\frac{\partial u}{\partial x} = \nu\frac{\partial^2 u}{\partial x^2},$$

where $u(x, t)$ is the velocity field, and ν is the viscosity coefficient.

Diffusion Equation The diffusion equation includes a time-dependent source term and is defined over the spatial domain $x \in [-1, 1]$ and temporal interval $t \in [0, 1]$. The initial condition is specified as $u(x, 0) = \sin(\pi x)$, with Dirichlet boundary conditions $u(-1, t) = 0$ and $u(1, t) = 0$. The diffusion equation is expressed as

$$\frac{\partial u}{\partial t} - \frac{\partial^2 u}{\partial x^2} = e^{-t}\left(\sin(\pi x) - \pi^2 \sin(\pi x)\right),$$

where $u(x, t)$ is the solution.

Poisson Equation The Poisson equation is defined over the spatial domain $x \in [0, 1]$ and $y \in [0, 1]$. The Poisson equation is expressed as

$$\frac{\partial^2 u}{\partial x^2} + \frac{\partial^2 u}{\partial y^2} = f(x, y),$$

where $u(x, y)$ is the solution, and $f(x, y)$ is the source term given by

$$f(x, y) = 2\pi^2 \sin(\pi x)\sin(\pi y).$$

C.2 EFFECT OF ACTIVATION FUNCTION ON PINN

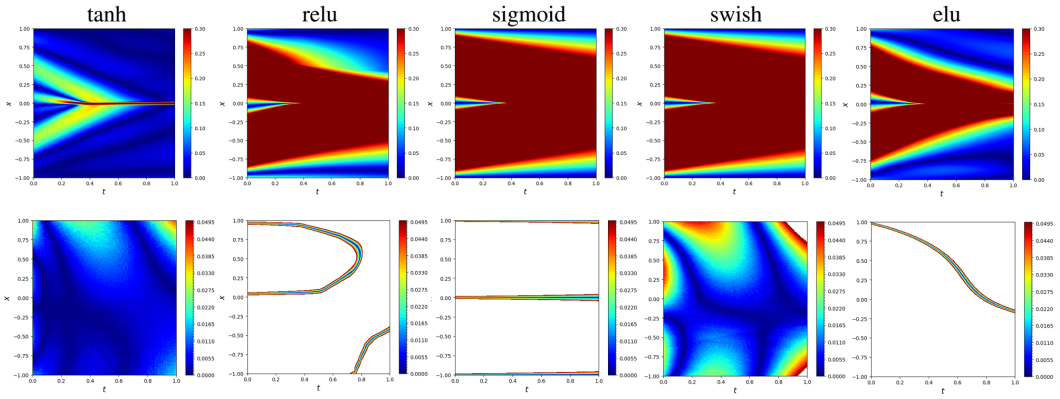

Figure 14: Absolute error for **(upper row)** the Burgers' equation and **(lower row)** the diffusion equation with varying activation functions. The FFNN consists of 30 hidden layers (32 nodes each) and is trained for 300 iterations using Adam, followed by 300 iterations using L-BFGS. Values outside the color bar range are represented in white.

We experimentally demonstrated that the absolute error between the exact solution and the PINN-predicted solution is smaller when using the tanh activation compared to ReLU, sigmoid, swish (Ramachandran et al., 2017), and elu activations (Clevert, 2015) in Figure 14. For the Burgers' and diffusion equations with a 30-hidden-layer architecture (32 nodes per layer), the PINN with tanh activation provided the closest approximation to the exact solution.

C.3 σ_z FOR BURGERS' EQUATION

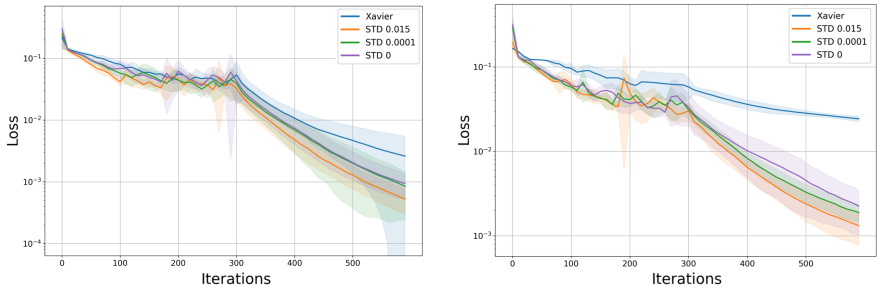

(a) Same dimension

(b) Varying dimensions

Figure 15: Here, STD refers to σ_z. (a) shows the PINN loss for the Burgers' equation, using an FFNN with 30 layers and 32 nodes in each hidden layer. (b) shows the PINN loss for an FFNN with 30 layers, where the hidden layers alternate between 64 and 32 nodes, repeated 15 times. Each experiment was repeated 10 times with different random seeds.

C.4 ABSOLUTE ERROR FOR BURGERS' EQUATION

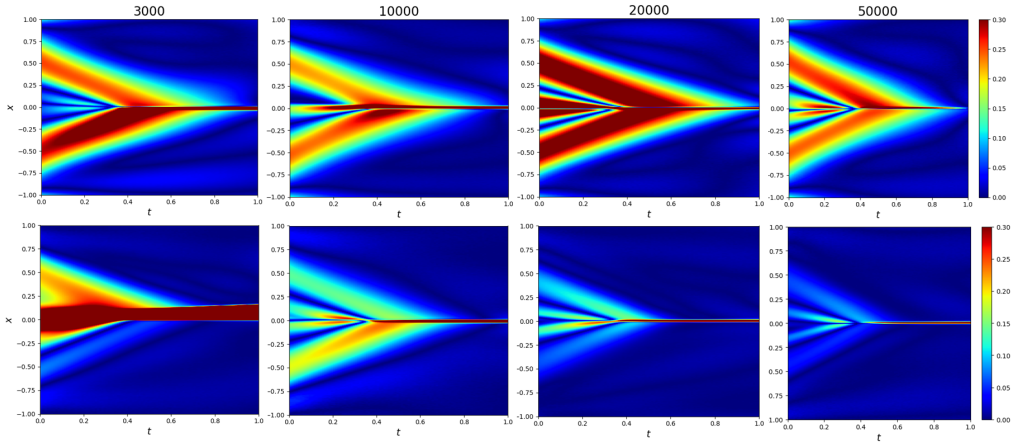

Figure 16: Absolute error between the exact solution and the PINN-predicted solution for the Burgers' equation with varying numbers of collocation points (3000, 10000, 20000, 50000) using **(upper row)** Xavier and **(lower row)** the proposed initialization. The FFNN has 30 hidden layers (32 nodes each) and is trained for 300 iterations using Adam followed by 300 iterations using L-BFGS.

D EXAMPLES OF THE MATRIX $\mathbf{D}^\ell$

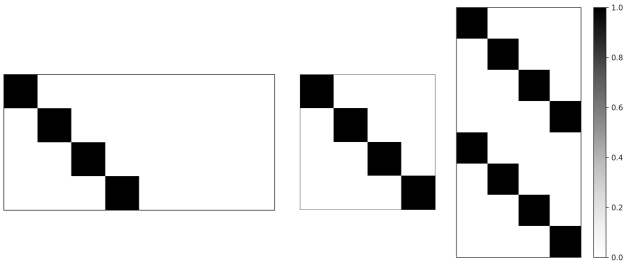

Figure 17: Examples of the matrix $\mathbf{D}^\ell \in \mathbb{R}^{N_\ell \times N_{\ell-1}}$ in Section 3.2 with $N_\ell = 4, N_{\ell-1} = 8$ (left), $N_\ell = 4, N_{\ell-1} = 4$ (middle), and $N_\ell = 8, N_{\ell-1} = 4$ (right), respectivley.

E A SIMPLE EXPERIMENT ON SWISH

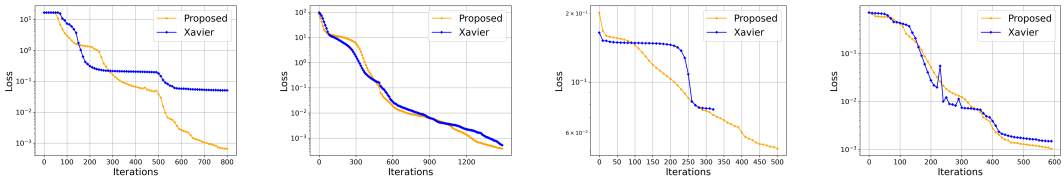

(a) Diffusion equation (b) Poisson equation (c) Burgers' equation (d) Allen-Cahn equation

Figure 18: PINN loss for a Swish FFNN with (a) 20 hidden layers, each containing 32 nodes, and (b), (c) 3 hidden layers, each containing 3 nodes, and (d) 10 hidden layers, each containing 32 nodes.